Journal of Umm Al-Qura University for Applied Sciences (2024) 10:211–224
https://doi.org/10.1007/s43994-023-00093-y

ORIGINAL ARTICLE

Quantifying AMPARs with ^{99m}Tc-omberacetam: a novel diagnostic radiotracer for ischemic stroke

Hala F. Azhari[1] · **Abdelgawad M. Hashem**[2]

Received: 22 August 2023 / Accepted: 20 October 2023 / Published online: 24 November 2023

Abstract

Synaptic trafficking of α-amino-3-hydroxy-5-methyl-4-isoxazole propionic acid receptors (AMPARs) is thought to cause excitotoxicity brain ischemia. However, given the current inability to quantify AMPARs density in live human brains, clinical translation has been limited. In this study, in vivo and in vitro experiments were conducted to evaluate the factors affecting omberacetam drug labeling with technetium-99m as a potential radiotracer of AMPARs in brain imaging. Healthy Swiss albino mice (adult male; $n = 25$; weight 25–30 g; age 10–14 weeks) underwent Shimadzu modeling, followed by a random intravenous injection of ^{99m}Tc-omberacetam (0.2 mL, 3.7 MBq), which was subsequently radiosynthesized in the brain-targeting AMPARs utilizing a single-photon emission computed tomography nuclear neuroimaging. Under optimal conditions, ^{99m}Tc-omberacetam with a highest radiochemical purity of 98.9% was obtained with an optimum binding (energy = − 82.3 kcal/mol) to brain AMPARs and was stable in human serum for > 24 h. A high brain uptake was noted within a time window of 15–60 min. At 5 min, this signal uptake was 8.9 ± 0.1% of the injected dose per gram (ID/g), crossing the blood–brain barrier and surpassing the uptake of commercially available brain perfusion imaging agents such as ^{125}I-iododomperidone (5.6% ID/g at 5 min) in mice, ^{99m}Tc-HMPAO (2.25% ID/g at 2 min) in rats, and ^{99m}Tc-ECD (4.7% ID/g at 6 h) in humans. This study is the first to show the feasibility of ^{99m}Tc-omberacetam radiotracing for human brain imaging. This could be a novel diagnostic and therapeutic neuroprotective target for the hyperacute stage of ischemic stroke.

✉ Hala F. Azhari
hfazhari@uqu.edu.sa

Abdelgawad M. Hashem
abdelgawad.hashem@bue.edu.eg

[1] Department of Pharmacology and Toxicology, Faculty of Medicine and Pharmacy, College of Medicine and Pharmacy, Umm Al-Qura University, Al-Ta'eef Road, P.O. Box 13578, 24243 Makkah, Saudi Arabia

[2] Department of Microbiology and Immunology, The British University in Egypt, El Sherouk 11837, Egypt

Graphical abstract

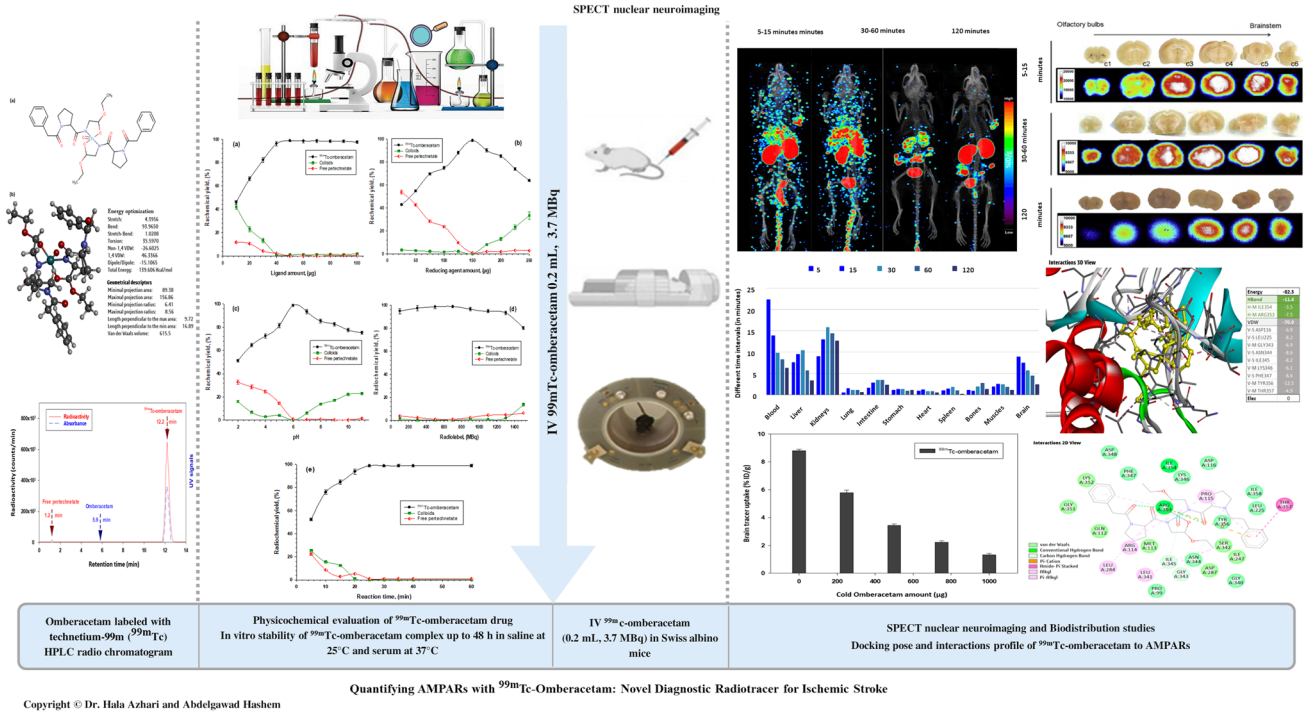

Keywords Omberacetam · α-Amino-3-hydroxy-5-methyl-4-isoxazole propionic acid receptors · Technetium-99m · Blood–brain barrier · Single-photon emission computed tomography nuclear neuroimaging · Stroke

1 Introduction

Stroke is the second most common cause of death worldwide, with 5 million deaths occurring annually [1]. It is estimated that up to two million neurons are lost every minute if reperfusion treatment is delayed from the time of stroke onset [2]. During ischemic stroke, disruption of blood supply induces anaerobic metabolism of glucose, resulting in lactic acid accumulation. Secondary hypometabolism [3] leads to a vicious cycle of worsening acidosis [4]. The α-Amino-3-hydroxy-5-methyl-4-isoxazole propionic acid receptor (AMPAR) dysfunction causes imbalances between inhibitory and excitatory synapses, thereby accelerating brain injury-induced neural death [5]. Synaptic trafficking [6] of AMPARs is believed to underlie neuronal plasticity [7], restricting AMPAR synaptic delivery that induces oxygen deprivation and leads to excitotoxic brain ischemia. After a few hours, the blood–brain barrier (BBB) integrity is compromised, triggering the final transition from ischemia to infarction to hemorrhagic transformation, thereby increasing the risk of recurrent stroke and mortality [8]. However, during the early hyperacute stage (4.5 ± 2 h) [9] of an ischemic stroke, some of the ischemic penumbral tissue may be saved if the cerebral blood flow (CBF) is swiftly restored. Thus, AMPAR is a neuroprotective interventional target for hyperacute ischemic stroke [10].

Clinical translation has been minimal, as no clinically approved technique to quantify AMPAR density in the human brain is available [11]. Several potential AMPAR tracers have been developed; however, none have reached clinical practice owing to low specific binding, low brain uptake, and rapid clearance [12]. Single-photon emission computed tomography (SPECT) nuclear neuroimaging has become a clinical diagnostic and research modality [13]. It provides a helpful noninvasive nuclear neuroimaging tool that increases our understanding of stroke pathogenesis and stroke-induced neurodegenerative disorders [14] through the qualification of sophisticated brain biological pathways, assessment of biochemical processes [15], in vivo characterization, and real-time visualization [16] for central nervous system drug development [17].

Omberacetam, a synthetic psychostimulatory molecule based on the endogenous neuropeptide cyclopropylglycine [18], is a neuroprotective drug for brain ischemia. Omberacetam, which has nootropic properties, can serve as a marker for brain imaging as it readily crosses the BBB [19] and produces its effect by modulating AMPARs [20]. Omberacetam is a selective agonist of AMPARs with a half

maximal inhibitory concentration of 6.4 ± 0.2 µM, while being 1000-fold as potent as piracetam [21]. Radiolabeled omberacetam may assist in further elucidating the molecular basis of brain ischemia as a novel diagnostic and therapeutic tool for the visualization and quantification of AMPARs in living humans.

The aims of this study were: (1) investigating omberacetam radiolabeling with gamma-emitter technetium-99m in animal modeling; (2) quality control, preparation, synthetization, and characterization of the non-radioactive rhenium analog ^{99m}Tc-omberacetam; (3) physicochemical evaluation of ^{99m}Tc-omberacetam to identify AMPAR binding sites in the brain for in vitro radiochemical stability; (4) study ^{99m}Tc-omberacetam biodistribution and clearance; (5) ^{99m}Tc-omberacetam blocking study; and (6) evaluation of its use as a potential radiotracer for brain imaging by determining the radiochemical purity and partition coefficient. Additionally, we hypothesized that using gamma-emitter technetium-99m would increase the omberacetam radiolabeling trace in healthy Swiss albino brain mice.

2 Results

2.1 Optimization of the ^{99m}Tc-omberacetam radiolabeling reaction

To achieve the maximum radiochemical yield (RCY) of ^{99m}Tc-omberacetam, the effects of different labeling parameters were optimized and studied (Fig. 1).

2.1.1 Effect of the ligand

A low omberacetam amount (10 µg) lead to a low RCY of 46.1 ± 1.6%, with approximately 12% colloid formation as the main impurity. As all reduced technetium was transformed to reduced hydrolyzed technetium colloids, the concentration of the ligand was not sufficient for complex formation. However, a 98.9 ± 1.1% maximum RCY was achieved when using 50 µg of concentrated ligand. Additional increases of the omberacetam amount had an insignificant impact on the RCY (Fig. 1a).

2.1.2 Effect of the reducing agent

When preparing the radiopharmaceutical technetium-99m compound, the most used reduced agent is stannous chloride dihydrate ($SnCl_2{\cdot}2H_2O$) [22]. It reduces the radiolabeling source eluted from the molygenerator (+7, pertechntate ions) to a more reactive, lower oxidation state. The study findings showed that when using a low amount of (25 µg) $SnCl_2{\cdot}2H_2O$, a low RCY of 42.8 ± 0.7% was obtained, suggesting that the $SnCl_2{\cdot}2H_2O$ content was insufficient to lower the pertechnetate ion concentration. With an increase in the amount of $SnCl_2{\cdot}2H_2O$, however, the yield gradually increased until reaching the most effective amount (150 µg), with an RCY of 98.9 ± 1.1%. When the reducing agent concentration was further increased, the RCY gradually decreased, which was as a result of undesired oxidized and hydrolyzed colloids formation (Fig. 1b).

2.1.3 Effect of the pH

The pH of a reaction is a factor that needs to be critically controlled as it impacts the labeled complex stability. Optimal radiochemical conversion was altered significantly by altering the pH from a strongly acid media to a strongly basic media (Fig. 1c). A pH of 6 resulted optimal, which may in part reflect the ^{99m}Tc-omberacetam complex stability (98.9 ± 1.1%). At pH of 2, free pertechnetate appeared to be the predominant species (32.8 ± 1.8%), while the RCY (51.1 ± 1.2%) was relatively low. Thus, increasing the pH above the optimum value decreased RCY to 75.2 ± 0.4% and 82.6 ± 1.8% at pH 11 and 9, respectively, with stannous hydroxide colloid formation being the predominant species.

2.1.4 Effect of the radiometal

To determine the optimum pertechnetate megabecquerels (MBq) for reconstitution, different radioactivity levels, 100–1500 MBq, were used. The feasibility and the complex stability in the presence of an additional quantity of pertechnetate were investigated using the same vial aiming to decrease the costs of imaging. The study findings showed that the best radioactivity was 700 MBq (Fig. 1d). Additionally, it was confirmed that radioactivity within a range of 300–900 MBq is feasible, as the complex is stable to radiolysis.

2.1.5 Reaction time

At 37 °C, an RCY of 76 ± 1.8% was reached at 10 min. Its maximum, 98.9 ± 1.1%, was reached when the reaction lasted 25 min. Subsequently, for reactions spanning > 1 h, the RCY remained stable and unchanged (Fig. 1e).

2.2 Quality control, preparation, synthesis, and characterization of ^{99m}Tc-omberacetam

In the omberacetam structure, the existence of nitrogen and oxygen donating atoms enables increased labeling with the transition metal technetium-99m (Fig. 2). At pH 6 and 25 min of reaction time, mixing 50 µg omberacetam with pertechnetate at approximately 350 MBq and 1 µg/µL of $SnCl_2{\cdot}2H_2O$ allowed for an RCY 98.9 ± 1.1% for ^{99m}Tc-omberacetam complex formation.

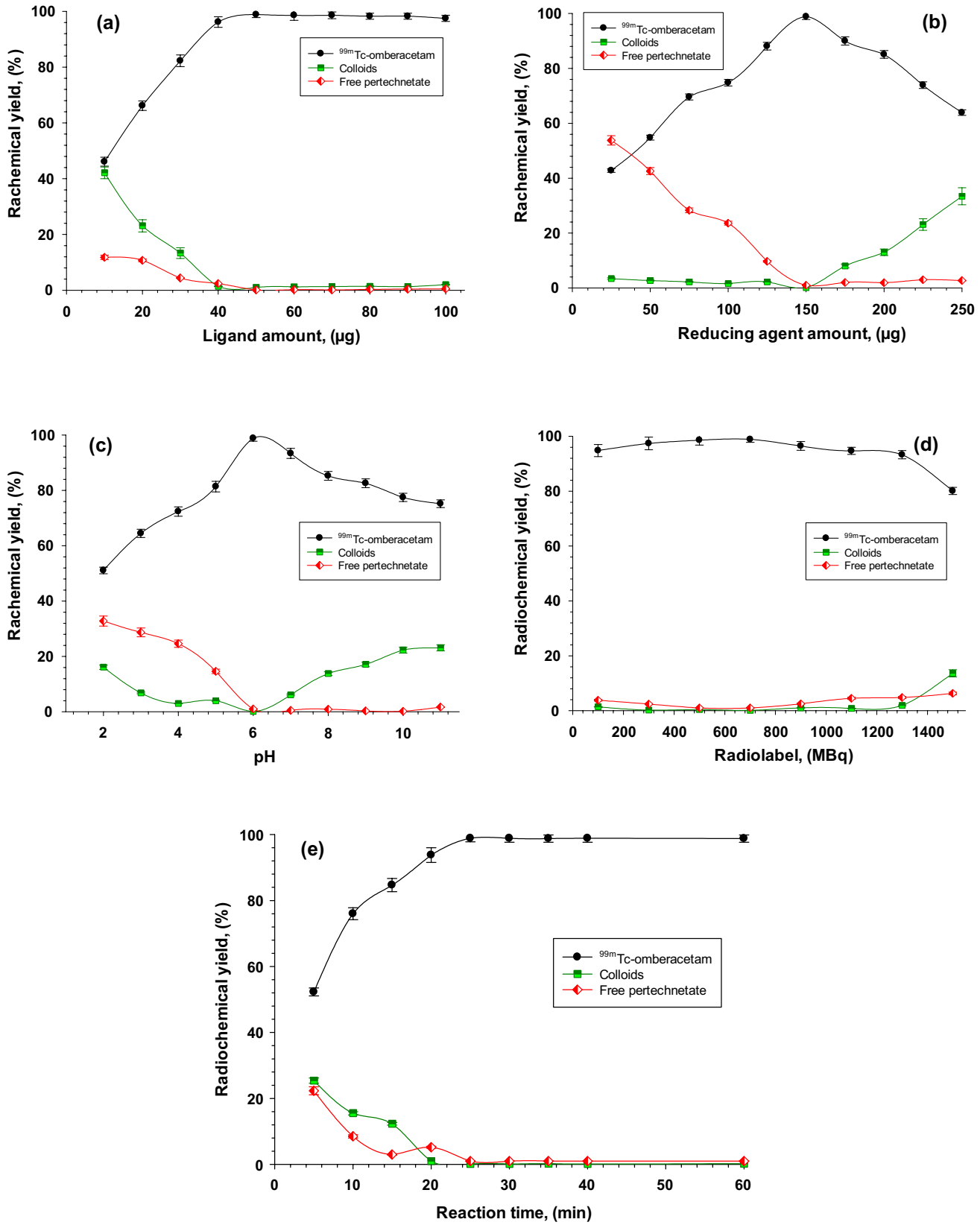

Fig. 1 Effect of **a** omberacetam; **b** stannous chloride dihydrate; **c** pH; **d** pertechnetate; and **e** reaction time on the radiochemical yield of the ^{99m}Tc-omberacetam complex

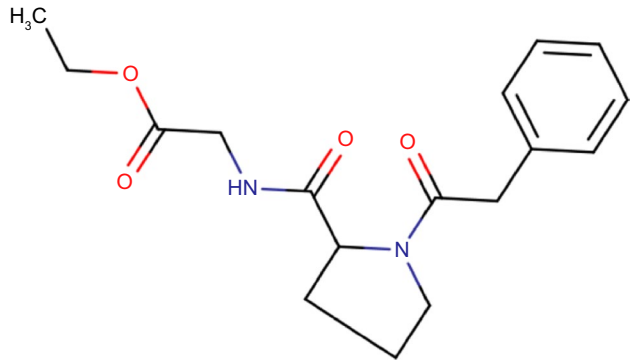

Fig. 2 Chemical structure of omberacetam

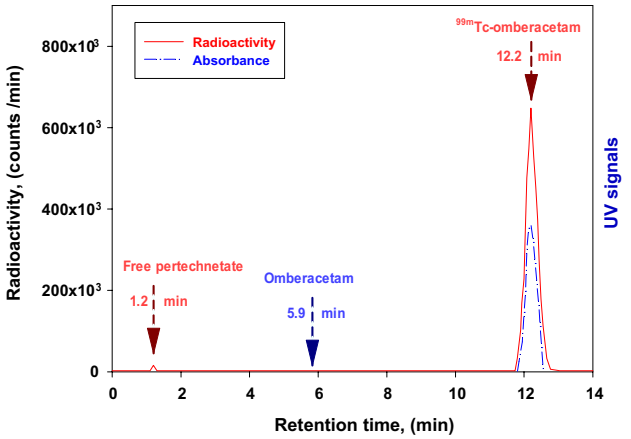

Fig. 3 The high-performance liquid radiochromatogram of the ^{99m}Tc-omberacetam complex

The purity of the radiochemical-labeled ^{99m}Tc-omberacetam was evaluated using the High-performance liquid chromatography (HPLC) and the silica gel impregnated thin layer chromatography (SG-TLC) techniques. When an water:ethanol:ammonium hydroxide [5:2:1] was used as the mobile phase, only the ($^{99m}TcO_2{\cdot}nH_2O$) colloids remained near the origin (R_f = 0–0.1), while the complex, free pertechnetate, and the solvent front (R_f = 0.8–1.0) migrated. In SG-TLC, however, when normal saline was used as the mobile phase, ^{99m}Tc-omberacetam complex and ($^{99m}TcO_2{\cdot}nH_2O$) colloids remained near the origin (R_f of 0–0.1), whereas the ($^{99m}TcO_4^-$) free pertechnetate moved with the solvent front (R_f of 0.8–1.0).

2.2.1 HPLC analysis and purification

The HPLC chromatogram of the reaction mixture showed two distinct peaks at 12.2 min and 1.2 min retention times, corresponding to ^{99m}Tc-omberacetam complex and the free pertechnetate, respectively. In the UV channel, the unlabeled omberacetam peak was detected at 5.9 min (Fig. 3).

A rhenium analog was synthesized and characterized to clarify the structure of the technetium-labeled complex. Element analysis results revealed the following compositions: C, 48.07%; H, 5.28%; N, 6.70%; O, 17.15%; and Re, 22.22%. The percentage results for the empirical formula ($C_{34}H_{44}N_4O_9Re$) were C, 48.68%; H, 5.29%; N, 6.68%; O, 17.16%; and Re, 22.20%. The ^{1}H NMR (500 MHz, CD Cl_3) spectrum showed peaks at the following δ ppm: 1.2 (s, 6 H), 1.93 (s, 2 H), 1.98 (s, 2 H), 2.03 (s, 2 H), 2.26 (s, 2 H), 3.22 (s, 2 H), 3.35 (s, 2 H), 3.48 (s, 2 H), 3.58 (s, 2 H), 3.64 (s, 2 H), 3.72 (s, 2 H), 3.76 (s, 2 H), 3.88 (s, 2 H), 4.55 (s, 2 H), 5.36 (s, 2 H), 6.95 (s, 4 H), 7.21 (s, 4 H), 7.22 (s, 2 H); whereas the ^{13}CNMR spectrum of the $CDCl_3$ (500 MHz) complex exhibited peaks at the following δ ppm: 15.24 (CH_3 aliphatic, $P_{22,}$ P_{44}), 25.18 (CH_2 cyclic, $P_{12,}$ P_{34}), 28.70 (CH_2 cyclic, $P_{13,}$ P_{35}), 40.95 (CH_2 cyclic, $P_{18,}$ P_{40}), 41.48 (CH_2 aliphatic, $P_{7,}$ P_{29}), 48.6 (CH_2 cyclic, $P_{11,}$ P_{33}), 61.99 (CH cyclic, $P_{14,}$ P_{36}), 6.32 (CH_2 aliphatic, $P_{21,}$ P_{43}), 80.82 (CH cyclic, $P_{19,}$ P_{41}), 127.29 (benzene, P_4, P_{26}), 127.99 (benzene, P_3, P_5, P_{25}, P_{27}), 129.19 (benzene, P_2, P_6, P_{24}, P_{28}), 133.88 (benzene, P_1, P_{23}), 162.57 (amide, P_{15}, P_{37}), and 168.09 (amide, P_8, P_{30}). The calculated methylsilane standard for the empirical formula $C_{34}H_{44}N_4O_9Re$ was 838.95, while the experimental value was 839.26. The mass spectrum [*m*/*z*: relative abundance] was as follows: 837: 0.57, 839: 1, 840: 0.38, 841: 0.09, 842: 0.02.

The structure of the ^{99m}Tc-omberacetam labeled complex was designed to ensure energy minimization (Fig. 4a). The theoretically calculated parameters and the software generated optimized geometries of the ^{99m}Tc-omberacetam complex three-dimensional structures are presented in Fig. 4b. ^{99m}Tc-omberacetam was expected to have a 2:1 ligand-to-metal ratio with an octahedral geometry.

2.3 Physicochemical evaluation of ^{99m}Tc-omberacetam

2.3.1 AMPARs binding

The iGemdock 2.1 software simulates Van der Waals, hydrogen bonding, and electrostatic interaction profiles within the ligands and receptors (Fig. 5). Using flexible docking interactions, it then reads the target coordinates of ligand molecule atoms and protein sequence and analyzes their molecular interactions, calculating the binding energy of protein binding site. The proposed interactions included hydrogen bonds between the essential amino acids and the complex (ILE354 and ARG353) and van der Waal's interactions with (ASP126, LEU255, GLY343, ASN344, ILE345, LYS346, PHE347, TYR356, and THR357).

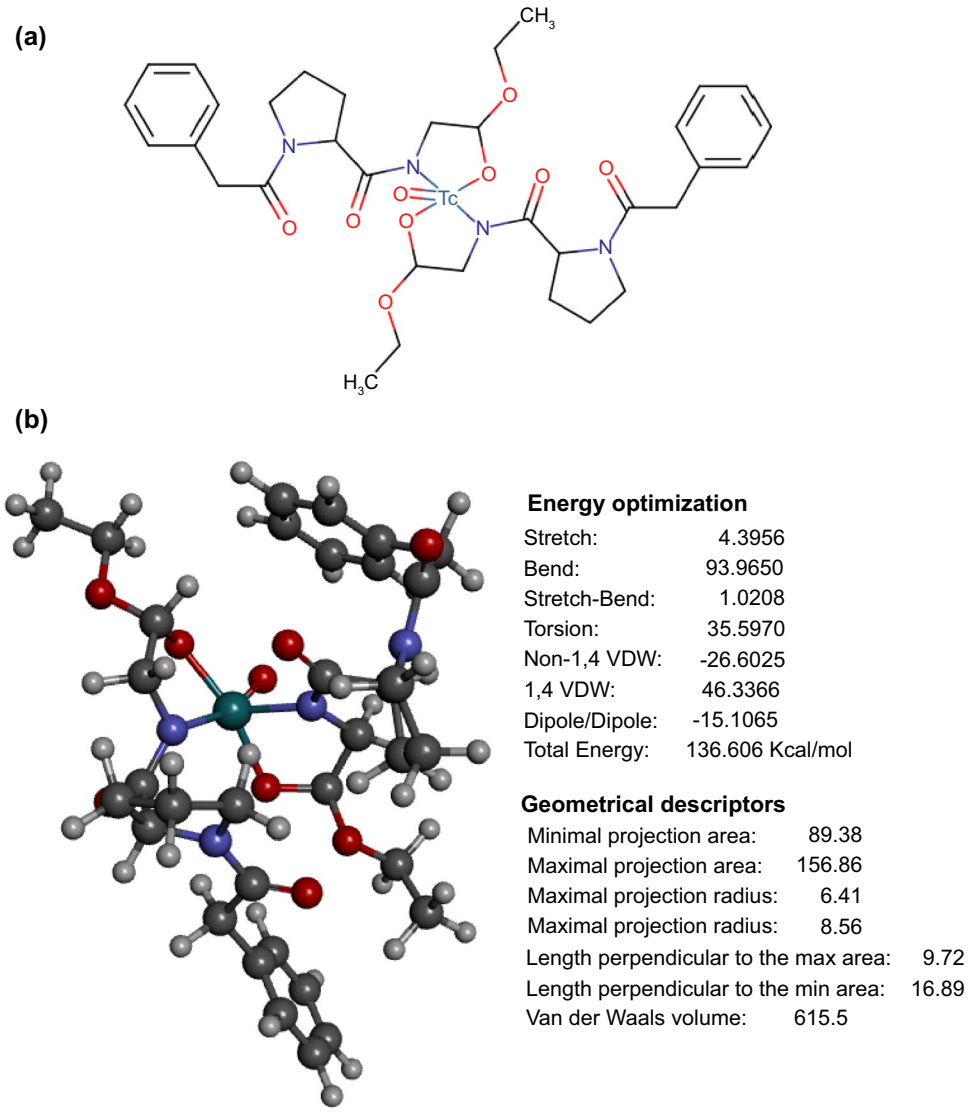

Fig. 4 **a** Chemical structure of the ^{99m}Tc-omberacetam complex; **b** optimized three-dimensional structure of ^{99m}Tc-omberacetam

2.3.2 In vitro radiochemical stability

The shelf life of ^{99m}Tc-omberacetam was studied to determine the time after reconstitution in which the labeled drug remains suitable for human use. Figure 6 indicates that technetium-99m-labeled omberacetam remained stable for up to 40 h at room temperature without significant byproducts that could interfere with the imaging process or lead to accumulation of radiotracer in non-target organs.

In the presence of serum, the stability of the in vitro labeled ^{99m}Tc-omberacetam was also examined at 37 °C. For up to 24 h, the complex demonstrated a stable profile indicating that it was suitable for administration to humans during this period. However, within 48 h the purity of the radiochemical reduced to 77.7 ± 0.9%, probably as a result of interactions with serum components.

2.4 ^{99m}Tc-omberacetam biodistribution and clearance

In vivo uptake of ^{99m}Tc-omberacetam was investigated; SPECT imaging revealed a rapid radiotracer distribution throughout the various tissues and body organs of the Swiss albino mice (Table 1).

The pharmacokinetic profile of ^{99m}Tc-omberacetam, a potential radiopharmaceutical, was assessed at different time intervals. At 5 min p.i., the blood uptake (22.3 ± 0.5% ID/g) was initially high but slowly decreased within 120 min p.i. to 6.2 ± 0.2% ID/g, likely due to binding to plasma proteins. The liver showed ID/g relatively high uptake of 10.4 ± 0.7% at 30 min p.i., which might result from hepatic omberacetam metabolization. Whereas the omberacetam labeled drug was mainly

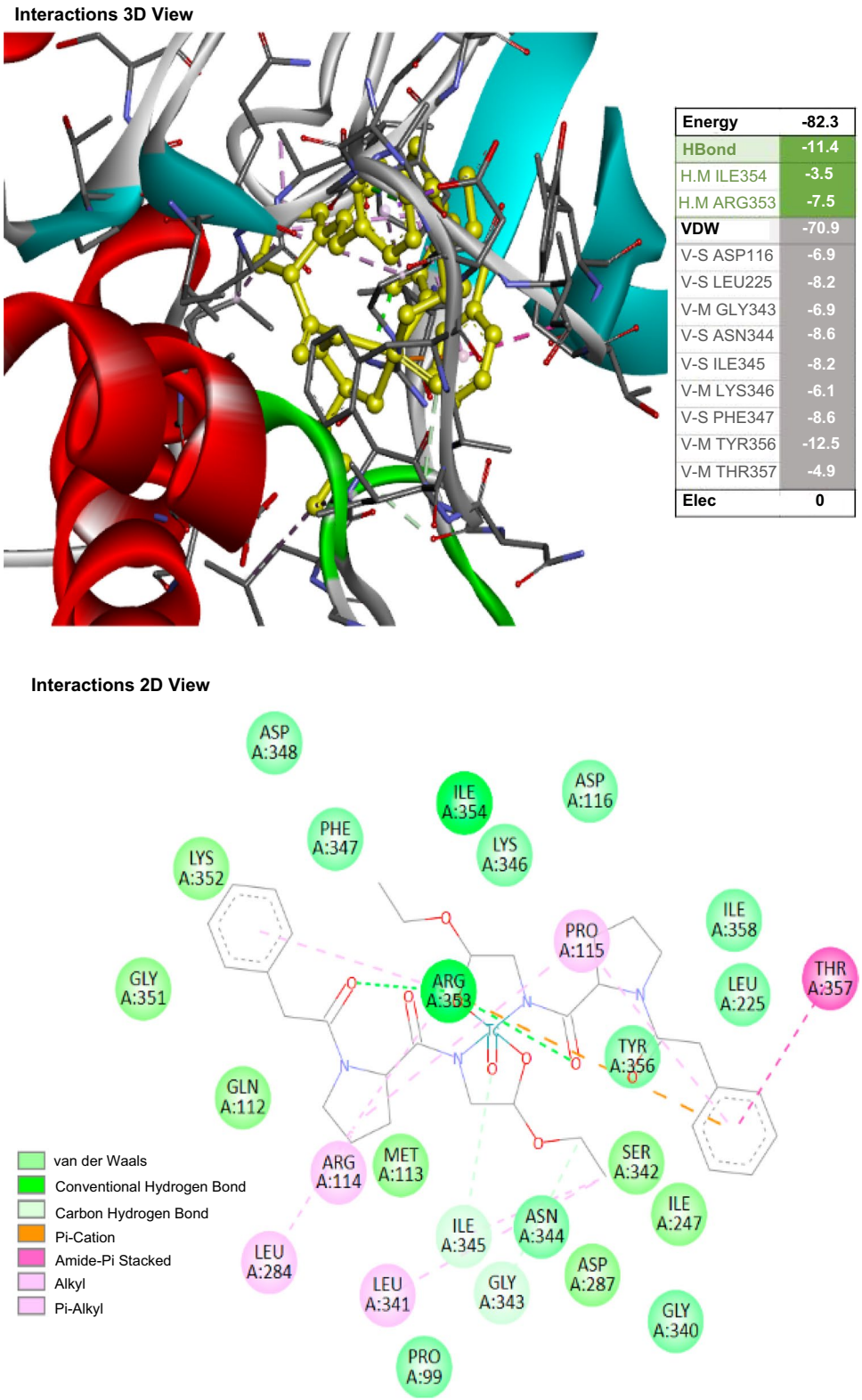

Fig. 5 Interaction views of the docking position of ^{99m}Tc-omberacetam to the target α-amino-3-hydroxy-5-methyl-4-isoxazole propionic acid brain receptors

excreted by the kidneys and, consequently, with time, the uptake increased to an ID/g of 15.8 ± 0.2% and remained high over time in comparison to that in further body organs. At 5 min p.i., the ^{99m}Tc-amberacetam had highly ID/g accumulated in the brain (8.9 ± 0.1%); thereafter, the uptake of ID/g levels decreased to 7.4 ± 0.2, 5.7 ± 0.2, 4.5 ± 0.1, and 2.4 ± 0.1% at 15, 30, 60, and 120 min p.i., respectively. Additionally, the brain to blood ratio was

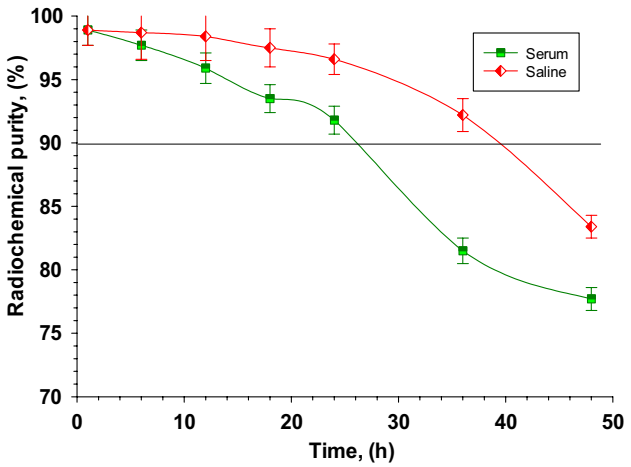

Fig. 6 In vitro radiochemical stability of the ^{99m}Tc-omberacetam complex up to 48 h in saline at 25 °C and serum at 37 °C

Table 1 ^{99m}Tc-omberacetam complex biodistribution profile in different organs of Swiss albino mice

Tissues/organs	^{99m}Tc-omberacetam injected dose per gram uptake at different times				
	5 min	15 min	30 min	60 min	120 min
Heart	0.9 ± 0.0	1.2 ± 0.0	0.8 ± 0.0	0.8 ± 0.0	0.5 ± 0.0
Lungs	0.5 ± 0.1	1.5 ± 0.2	1.1 ± 0.1	1.1 ± 0.0	0.6 ± 0.0
Liver	7.5 ± 0.1	9.5 ± 0.2	10.4 ± 0.0	5.7 ± 0.3	3.4 ± 0.1
Stomach	1.1 ± 0.1	1.3 ± 0.0	1.3 ± 0.0	0.9 ± 0.1	1.1 ± 0.0
Spleen	1.0 ± 0.0	1.4 ± 0.0	1.8 ± 0.0	1.0 ± 0.0	0.2 ± 0.0
Intestine	1.6 ± 0.1	2.8 ± 0.2	3.4 ± 0.1	3.4 ± 0.3	2.3 ± 0.1
Muscles	1.9 ± 0.1	2.5 ± 0.0	2.4 ± 0.0	1.8 ± 0.1	1.1 ± 0.1
Bones	1.1 ± 0.1	0.9 ± 0.0	1.9 ± 0.1	2.7 ± 0.2	1.3 ± 0.1
Brain	8.9 ± 0.1	7.4 ± 0.2	5.7 ± 0.2	4.5 ± 0.1	2.4 ± 0.1
Kidneys	9.0 ± 0.1	12.9 ± 0.3	15.8 ± 0.2	14.4 ± 0.4	12.6 ± 0.2
Blood	22.3 ± 0.5	13.9 ± 0.2	9.8 ± 0.1	8.3 ± 0.8	6.2 ± 0.2

Mean ± standard error (mean of five experiments, with five mice per experiment)

Vial content at a pH 6: 150 µg stannous chloride dihydrate, 50 µg omberacetam, and ~ 700 MBq technetium 99m; the reaction mixture was kept for 25 min at 25 °C

calculated to assess the relative uptake in the brain compared to that in the bloodstream. The %ID/g uptake brain to blood ratios were 0.39, 0.53, 0.58, 0.54, and 0.38 at 15, 30, 60, and 120 min p.i., respectively. The radioactivity in the other organs was within the normal range (Fig. 7).

The radiotracer clearance per unit time followed first-order elimination kinetics. As shown in the clearance study results (Fig. 8), the elimination rate constant was 0.63 h^{-1}.

2.5 ^{99m}Tc-omberacetam blocking study

Varying amounts of unlabeled omberacetam (0–1000 µg) were used to dosage mice before the radiotracer injection. After pre-dosing, the ^{99m}Tc-omberacetam brain uptake at 5 min was determined. The radiotracer uptake was blocked by the unlabeled omberacetam in the brain in a dose-dependent manner, suggesting that the accumulation of radiotracer reflects the interaction with the target protein (Fig. 9).

2.6 Partition coefficient

The partition coefficient is an important measure for the evaluation of radiotracer candidates. Furthermore, it has a major influence on the pharmacological action, as it conveys the ease with which a drug binds to the target receptor in order to reach its target within the body. It also controls the pharmacokinetics of drugs, including its absorption, body distribution, and the rate at which they are metabolized and excreted. We found that the penetration of ^{99m}Tc-omberacetam complex through the BBB to target the brain was optimal when the partition coefficient was between 1.5 and 2.7. We found that the determined log *P* value of the ^{99m}Tc-omberacetam complex was 2.52 ± 0.2.

3 Discussion

The novel findings in this study are as follows: (1) radiosynthetization of omberacetam with technetium-99m forms a single ^{99m}Tc-omberacetam labeled complex with a RCY peak at 12.2 min retention time to target AMPARs in the brain; (2) at optimum conditions, the radiocomplex was obtained at a high RCY of 98.9 ± 1.1%; (3) 50 µg of omberacetam solution was sufficient to interact with all the reduced technetium-99m generated using $SnCl_2{\cdot}2H_2O$; (4) ^{99m}Tc-omberacetam remained stable for 24 h, indicating its suitability for humans administration during this period; (5) the determined log *P* value was 2.52 ± 0.2, indicating the lipophilicity of the radiotracer complex and its capability to cross the BBB; (6) the computer-generated docking position and interaction profile of ^{99m}Tc-omberacetam had an optimal binding energy of − 82.3 kcal/mol in the brain; and (7) the maximum uptake of radiotracer in the brain was 8.9 ± 0.1% ID/g, within an acute target window at 5 min, interestingly higher than that currently reported ID/g for brain perfusion imaging radiopharmaceuticals such as ^{99m}Tc-ECD (in humans of 4.9% p.i. at 6 h) [23], ^{125}I-iododomperidone (in mice of 5.6% p.i. at 5 min) [24], and ^{99m}Tc-HMPAO (in rats of 2.25% p.i. at 2 min) [25]. To the best of our knowledge, our results are the first to demonstrate the potential

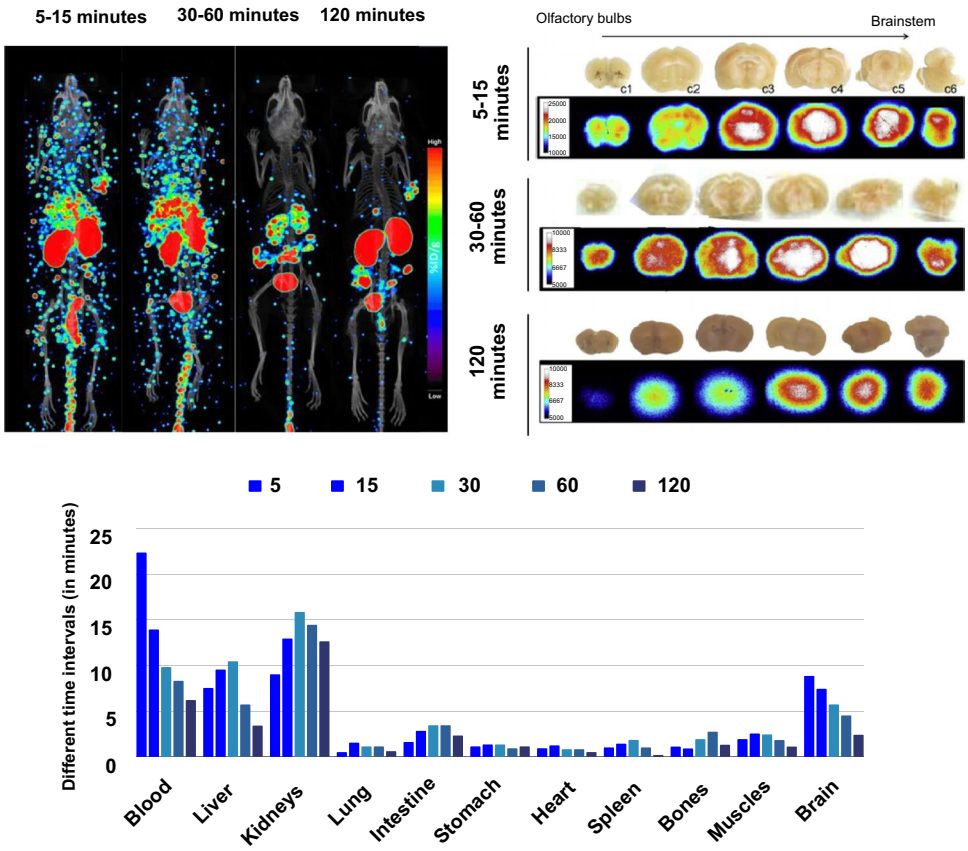

Fig. 7 Biodistribution of the ^{99m}Tc-omberacetam radioactivity complex, using SPECT nuclear neuroimaging, in various organs of Swiss albino mice at different time intervals (in minutes). SPECT, single-photon emission computed tomography

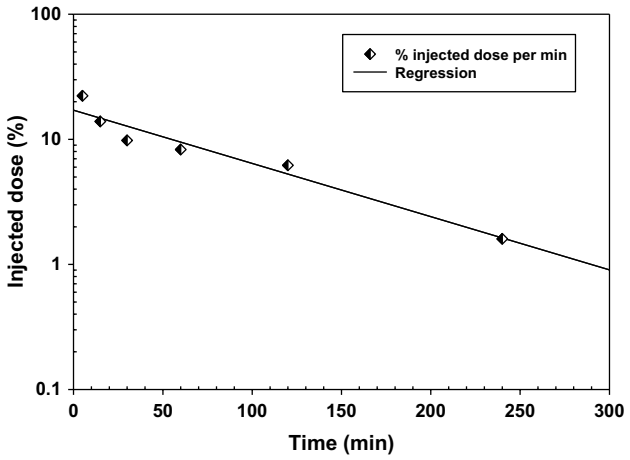

Fig. 8 Blood clearance of ^{99m}Tc-omberacetam in Swiss albino mice

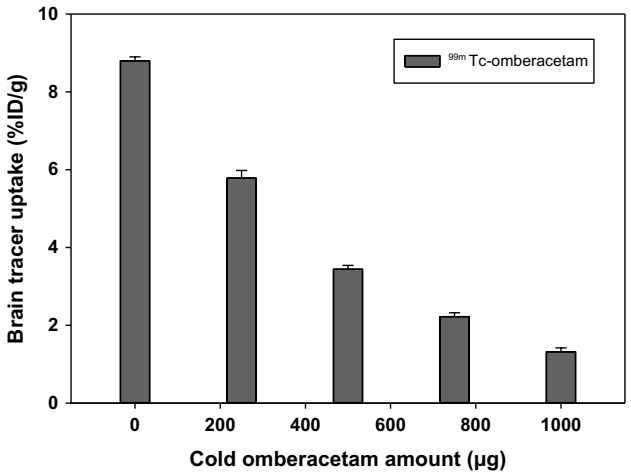

Fig. 9 Inhibition of ^{99m}Tc-omberacetam brain uptake in healthy Swiss albino at 5 min post-injection following pre-dosing with different amounts of unlabeled omberacetam

application of ^{99m}Tc-omberacetam as a radiotracer to quantity AMPAR for brain imaging diagnosis and may contribute to further radiopharmaceutical development research.

In the brain, the AMPARs are the predominant glutamate excitatory neurotransmitters [26] that mediate signal transmission at neuronal synapse. The neuronal cell interactions and the molecular and subcellular mechanisms underlying stroke [27] and stroke-induced neurodegenerative disorders [28] are poorly understood. Moreover, the brain ischemic penumbral tissue is a region with reduced regional CBF that is near the threshold for functional and morphological integrity maintenance [29], but with preserved oxygen

consumption. Although glutamate is thought to increase in the brain parenchyma within minutes of acute ischemic [30] and hemorrhagic strokes [31], penumbral brain tissue has the potential to recover if CBF is swiftly restored. Therefore, targeting AMPA glutamate receptors early after a post-ischemic stroke has the potential to ensure tissue rescue as an early hyperacute interventional therapy. Our study revealed that the ^{99m}Tc-omberacetam radiotracer, using a concentrated ligand with a low binding energy, demonstrated a maximum uptake within a short time, suggesting the presence of viable brain tissues that modulate AMPA glutamate receptors. It also showed that ^{99m}Tc-omberacetam may be an alternative and simple diagnostic and therapeutic radiotracer for the early hyperacute stage of ischemic stroke.

In acute ischemic stroke patients, prognostication of recovery using technetium-99m has been studied previously; however, this was performed for the labeling of metronidazole [32]. Technetium-99m-ethylene dicysteine-metronidazole (^{99m}Tc-EC-MN) was used in that study because it localizes to the hypoxic but viable brain tissue. Nevertheless, ^{99m}Tc-EC-MN was found to be a significant predictor of neurological deficits in the subacute phase, approximately the first 10.3 ± 2.5 days, in patients with acute ischemic stroke. Despite the significant uptake of ^{99m}Tc-EC-MN in that study, there was a discrepancy between the ethylene dicysteine-metronidazole and the ^{99m}Tc-ethyl cysteinate dimer (ECD) brain SPECT uptake, with a lower extraction coefficient observed in low flow ischemia and a low ECD trace retention in areas of hyperperfused infarct. Although the integrity of BBB could change within the first four days following acute ischemia [33]. Even so, ischemic stroke patients may not have salvageable tissue that can be treated, because the penumbral brain survival duration is likely to vary and would not persist during the 9 ± 3 days onset of the subacute stage of an ischemic stroke. However, omberacetam is a powerful antioxidant peptide analogue prescribed in Russia as a nootropic drug with neuroprotective pharmacokinetic and pharmacodynamic properties [34]. Additionally, omberacetam was radiosynthesized with ^{99m}Tc in this study as it protects the brain against early oxidative damage and is used against cognitive impairment in Alzheimer's disease [35].

The preparation and bioevaluation of ^{131}I-iodoomberacetam as a radiotracer have been recently reported in mice [36]. ^{131}I-iodoomberacetam was found to have the highest RCY of 98% brain uptake p.i. at 5 min using 100 µg chloramine-T as oxidative agent within a ~ 15 min retention time peak. At pH 5, the 96% complex purity was maintained in saline for two days, showing a 1.33 ± 0.12 log *P* value for its BBB lipophilicity; however, it underwent an 88% relative reduction in serum after one day. Instead, in this study, the blood to brain ratio showed that the optimal moment to use ^{99m}Tc-omberacetam as a radiotracer for a higher brain uptake. ^{99m}Tc-omberacetam with a 98.9 ± 1.1% purity p.i. at 5 min, stability up to 40 h in saline and > 24 h in human serum, showed the strongest AMPAR binding. Therefore, it is necessary to devise a diagnostic time window using ^{99m}Tc-omberacetam as a radiotracer for brain imaging to obtain an AMPARs ligand that not only allows its transport across the BBB but also facilitates its retention within a fixed distribution for long enough to allow SPECT brain imaging.

This experimental study, to our knowledge, is the first in which the radiosynthesis of ^{99m}Tc-amberacetam has been investigated for its potential use as a radiotracer to quantify AMPARs signal for brain imaging. This study has some limitations. The experiments were performed in healthy Swiss albino mice, and our results may not be directly transferable to other disease animal models. Therefore, further clinical studies on patients with acute ischemic stroke quantifying AMPAR using ^{99m}Tc-amberacetam may be needed to be further assess and determine the amount of viable tissue present, which may vary between infarct core and/or subtypes of cerebral ischemia, and to predict their neurological outcomes.

4 Methods and materials

4.1 Chemicals reagents and experimental studies

This study's experimental chemicals were of the highest grade of purity. Double distilled water, nitrogen purified, was used for dilution and dissolution. Omberacetam (Noopept; MW 318.37; ethyl 2 [[(2S) 1 (2 phenylacetyl) pyrrolidine 2 carbonyl] amino] acetate; Chem Science, New Jersey, U.S.A). The pertechnetate was eluted using a molygenerator supplied by ELUTEC (Brussels, Belgium). A Vario EL elemental analyzer (Chem Science, New Jersey, U.S.A.) was used for element analysis. Carbon 13 nuclear magnetic resonance (^{13}CNMR) spectroscopy and high-resolution nuclear magnetic resonance (^{1}HNMR) spectroscopy were performed utilizing a 500 MHz AMX Bruker spectrometer (Chem Science, New Jersey, U.S.A.) in CD Cl_3, an internal tetramethylsilane standard.

The animals used in the experiments were healthy Swiss albino mice (adult males; weight 25–30 g; aged 10–14 weeks) obtained from the Labeled Compounds Department Animal House, Atomic Energy Authority in Cairo, Egypt. Mice weighing < 25 g or > 30 g were excluded from the experiments. Mice were housed in metabolic cages, had access to water and food, and allowed to adapt for two weeks. Mice were randomly assigned to one of the study groups immediately after adaptation by drawing lots. All experimental assessments and analyzes were performed in a blind manner.

4.2 Outcome measures

The primary outcome was the labeling of the omberacetam drug. The secondary outcome measures to determine the optimal labeling reaction that affect the labeling yield under the following steps: (1) use of different amounts of the omberacetam ligand (5–50 µg), use of $SnCl_2{\cdot}2H_2O$ (25–250 µg) as a reducing agent, changes in the reaction medium of various pH values (2–11), radiometal activity of pertechnetate (100–1500 MBq), for different reaction times (5–40 min); (2) quality control, preparation, synthesis, and characterization of a non-radioactive rhenium analog (^{99m}Tc-omberacetam); (3) physicochemical evaluation of ^{99m}Tc-omberacetam (AMPAR binding site in the brain and in vitro radiochemical stability); (4) biodistribution and clearance studies; (5) blocking study; and (6) statistical analysis to determine the radiochemical purity and the partition coefficient. All of these factors were assessed using in vivo Swiss Albino experimental modeling and in vitro human serum endpoints.

4.2.1 Labeling of omberacetam

The effects of the different labeling parameters were analyzed and optimized. A mixture of $SnCl_2{\cdot}2H_2O$ (0.2 mL, 150 µg) and omberacetam (0.5 mL, 25 µg) was added to a phosphate buffer (0.1 M, pH 6) and maintained in a sterile vial in positive nitrogen pressure. Subsequently, an approximate solution of freshly eluted pertechnetate (350 MBq) was obtained from a molygenerator, added to the mixture, and incubated for 25 min at 37 °C.

4.2.2 Quality control, preparation, synthesis, and characterization of a non-radioactive ^{99m}Tc-omberacetam rhenium analog

To determine the structure of ^{99m}Tc-omberacetam, a cold labeling reaction was performed using potassium perrhenate [37]. In a sterile vial, omberacetam (2.5 mg, 7.8 µmol) was melted at (pH 6) in 10 mL phosphate buffer and stirred by ultrasonication for 10 min to dissolve it completely. $SnCl_2{\cdot}2H_2O$ of (2.6 mg, 11.4 µmol) and potassium perrhenate (1.1 mg, 3.9 µmol) were separately melted in a double distilled water purified with a minimal amount of nitrogen and were subsequently mixed together. After adjusting the pH to 6, the mixture was then added to the reaction vial that was incubated at 25 °C for 25 min. HPLC was used to purify and separate (re-omberacetam) the product. It was then characterized by ^{1}HNMR, ^{13}CNMR, high-resolution mass spectrometry, and elemental analysis.

4.2.2.1 HPLC analysis and purification HPLC was performed operating a Shimadzu model (Genzo Shimadzu Sr., Kyoto, Japan), equipped with LC-9A pumps, a radioisotope detector (Bioscan Inc., Washington, U.S.A.), and an UV spectrophotometer (-6ASPD, Shimadzu, Genzo Shimadzu Sr., Kyoto, Japan) detector; and a Rheodyne injector. Chromatography was performed on a particle size of 250 × 4.6 mm using a RP-18 column with a flow rate of 2.0 using a volume sample of 10 µL. To perform the elution, a mixture of water/acetonitrile/acetic acid (80:20:0.1%, v/v) was monitored with an UV wave detection at a range of 280–290 nm using mobile phase systems. To identify the ^{99m}Tc-omberacetam complex, HPLC confirmed that the radiolabeled omberacetam matched the non-radioactive rhenium-labeled omberacetam [38]. The ^{99m}Tc-omberacetam was co-injected with an analog of rhenium. The peaks retention time were then identified in the UV channel at a range of 280–290 nm and compared in the radiometric channel.

4.2.3 Physicochemical evaluation of ^{99m}Tc-omberacetam

4.2.3.1 AMPAR binding To evaluate the binding of ^{99m}Tc-omberacetam to the AMPARs, a docking study was performed [39]. The X-ray crystallographic structure of the target protein was imported from the Protein Data Bank RSCB (3KG2). The iGemdock 2.1 [40] software was used to investigate the most suitable binding position of ^{99m}Tc-Omberacetam by quantifying the binding site of AMPARs. The docking accuracy of the radiolabeled complex was assessed by allocating a target population size of 800 and one solution with 80 generations. The positions of the docked ligands with low-binding energies were then designated to analyze their interactions with the target protein residues.

4.2.3.2 In vitro radiochemical stability The stability of ^{99m}Tc-omberacetam complex was tested for 48 h at 37 °C. A saline solution (2 mL) was mixed with the complex (1 mL), and the 2 µL samples were withdrawn in triplicates after 1, 2, 4, 6, 12, 24, and 48 h and evaluated by the SG-TLC [41]. The percentage increase of colloids and free pertechnetate designated the dissociation of the labeled complex. A 1.8 mL sample of human serum was mixed with 0.2 mL of radiolabeled ^{99m}Tc-omberacetam and incubated for 48 h at 37 °C. Aliquots (2 µL) were withdrawn from the mixture at various time intervals, developed with water:ethanol:ammonium hydroxide (5:2:1) and saline, and analyzed by SG-TLC. Then, the in vitro stability percentage was calculated.

4.2.4 ^{99m}Tc-omberacetam biodistribution and clearance studies

The tail vein of mice was randomly injected intravenously with 0.2 mL of ^{99m}Tc-omberacetam (3.7 MBq). To reduce pain, suffering, and distress, mice were anesthetized with ketamine, post-injection (p.i.), at 5, 15, 30, 60, and 120 min

after tail vein injection, weighed, and dissected to determine tissue radiotracer distribution. Blood samples were collected via heart puncture. The major organs (heart, lungs, stomach, spleen, liver, intestine, brain, and kidneys) were collected and washed with normal saline twice, weighed, and analyzed for radiation activity using a ray of gamma counter using NaI Tl scintillation (Radio Corporation of America, Media Electronics, Westinghouse, U.S.A.).

4.2.5 ^{99m}Tc-omberacetam blocking study

Varying amounts, 0–1000 µg, of unlabeled omberacetam were administered intravenously to the mice for 10 min before the administration of radiotracer to block brain AMPARs. In the brain, radiotracer uptake percentage was determined 5 min after its injection ($n=5$).

4.3 Statistical analysis

For each group of experiments, descriptive statistics were used with a measure of variability. The number of mice per group required to reach a desired power of 0.800 was between four and six. Therefore, five experiments (five mice per set) were used for the biodistribution studies ($n=25$). All experiments for each factor were conducted and repeated in triplicates. The elimination rate constant of the radiotracer was calculated, and the results of the experiments were expressed as percentage of the tissue mean uptake of an injected dose per gram (% ID/g) and standard error (SE). When a one-way analysis of variance P value was <0.05, statistical differences were considered significant.

4.3.1 Radiochemical purity analysis

SG-TLC determined the radiochemical purity of ^{99m}Tc-omberacetam. Separate systems of developmental (water:ethanol:ammonium hydroxide [5:2:1] and saline) were employed [42] to determine the percentages of the labeled complexes, colloids, and loss pertechnetates. Aliquots (5 µL) of the reaction mixture were collected onto two strips of the SG-TLC (1.5 cm^2). In closed jars packed with nitrogen gas, the development was performed to shield the categorized spots from oxidization. The two radio-chromatograms were then dried, reduced into 1-cm slices, and calculated utilizing a gamma scintillation counter. The radiochemical purity percentage was determined following the subsequent equation:

$$\%labeled\ omberacetam = 100 - (\%\ colloid + \%\ loose\ pertechnetate)$$

4.3.2 Partition coefficient determination

The partition coefficient conveys the degree of drug lipophilicity. The categorized complex of the partition coefficient was determined using a formerly suggested approach for mild changes [43]. In short, freshly prepared ^{99m}Tc-omberacetam, was blended with phosphate buffer (0.025 M; pH 7.4) and organic solvent (n.octanol) in a centrifuge tube. At 37 °C, the mixture was vortexed for 5 min and then centrifugated at 8,000 rpm for 10 min. Eventually, 100 µL samples were collected from the aqueous and organic layers to different tubes and were counted via a properly-type gamma counter (SR7 Ratemeter Scalar, Nuclear businesses Ltd., USA). The experimental partition coefficient value was calculated and expressed as log P using the subsequent equation:

$$log\,P = log\frac{Radioactivity\ in\ organic\ layer}{Radioactivity\ in\ aqueous\ layer}$$

The ACD/NMR Processor V_{12} [44] software was used to predict the NMR structure and conduct the correlation analysis. The Ultra ChemBio3D [45] software was used to predict the geometrical-optimized three-dimensional model of ^{99m}Tc-omberacetam and to design its structure by energy minimization using Chemdraw Ultra 11.0 (PerkinElmer, Massachusetts, U.S.A.). The software iGemdock 2.1 [40] was used to evaluate the radiotracer binding to the AMPARs target brain site.

4.4 Reporting of the study results

The Checklist for Animal Research: Reporting of In Vivo Experiments [46] was followed in conducting and reporting of this study.

5 Conclusions

The ^{99m}Tc-omberacetam radiotracer, quantifying the brain AMPARs, can be a novel diagnostic and therapeutic tool for the early hyperacute stage of ischemic stroke. This radiotracer should be further assessed in acute ischemic stroke patients, using the results of this study to inform future trials designs.

Acknowledgements The authors thank the Deanship of Scientific Research at Umm Al-Qura University (UQU), Makkah, Saudi Arabia, and the Egyptian Labeled Compounds Department of the Egyptian Atomic Energy Authority, Cairo, Egypt for supporting this research works.

Author contributions All authors contributed to the study conception and design. Material preparation, data collection and analysis were

performed by Hala Azhari and Hashem Abdelgawad. The first draft of the manuscript was written by Hala Azhari and all authors commented on previous versions of the manuscript. All authors read and approved the final manuscript.

Funding This research was funded by the Deanship of Scientific Research at Umm Al-Qura University (UQU), Makkah, Saudi Arabia, grant code number (23UQU4290367DSR01N). This work was further sponsored by the Egyptian Labeled Compounds Department of the Egyptian Atomic Energy Authority, Cairo, Egypt. The study design, data collection, analysis, interpretation, or manuscript writing were all conducted independently from the funder and sponsor.

Data availability Original data and materials are available from the corresponding author upon reasonable request.

Declarations

Conflict of interest The authors declare that there is no conflict of interest.

Ethical approval The in vitro and in vivo experimental study design and protocols were carried out following the relevant guidelines and regulations of the Egyptian Labeled Compounds Department. Additionally, all experiments were approved by the Egyptian Animal Ethics Committee [EAEA/2022/188].

References

1. World Health Organization (2020) The top 10 causes of death. https://www.who.int/news-room/fact-sheets/detail/the-top-10-causes-of-death. Accessed 4 July 2023
2. Saver JL (2006) Time is brain-quantified. Stroke 37:263–266. https://doi.org/10.1161/01.STR.0000196957.55928.ab
3. Amin A, Choi SK, Galan M et al (2012) Chronic inhibition of endoplasmic reticulum stress and inflammation prevents ischaemia-induced vascular pathology in type II diabetic mice. J Pathol 227:165–174. https://doi.org/10.1002/path.3960
4. Anderson RE, Tan WK, Martin HS et al (1999) Effects of glucose and PaO_2 modulation on cortical intracellular acidosis, NADH redox state, and infarction in the ischemic penumbra. Stroke 30:160–170. https://doi.org/10.1161/01.str.30.1.160
5. Nguyen V, McQuillen PS (2010) AMPA and metabotropic excitoxicity explain subplate neuron vulnerability. Neurobiol Dis 37:195–207. https://doi.org/10.1016/j.nbd.2009.10.002
6. Beattie MS, Ferguson AR, Bresnahan JC (2010) AMPA-receptor trafficking and injury-induced cell death. Eur J Neurosci 32:290–297. https://doi.org/10.1111/j.1460-9568.2010.07343.x
7. Jitsuki S, Nakajima W, Takemoto K et al (2016) Nogo receptor signaling restricts adult neural plasticity by limiting synaptic AMPA receptor delivery. Cereb Cortex 26:427–439. https://doi.org/10.1093/cercor/bhv232
8. Saber H, Liebeskind DS (2021) Infarct progression in the early and late phases of acute ischemic stroke. Neurology 97:S60–S67. https://doi.org/10.1212/wnl.0000000000012795
9. Kuroda S, Siesjö BK (1997) Reperfusion damage following focal ischemia: pathophysiology and therapeutic windows. Clin Neurosci 4:199–212
10. Chang PK, Verbich D, McKinney RA (2012) AMPA receptors as drug targets in neurological disease–advantages, caveats, and future outlook. Eur J Neurosci 35:1908–1916. https://doi.org/10.1111/j.1460-9568.2012.08165.x
11. Miyazaki T, Nakajima W, Hatano M et al (2020) Visualization of AMPA receptors in living human brain with positron emission tomography. Nat Med 26:281–288. https://doi.org/10.1038/s41591-019-0723-9
12. Oi N, Tokunaga M, Suzuki M et al (2015) Development of novel PET probes for central 2-amino-3-(3-hydroxy-5-methyl-4-isoxazolyl)propionic acid receptors. J Med Chem 58:8444–8462. https://doi.org/10.1021/acs.jmedchem.5b00712
13. Israel O, Pellet O, Biassoni L et al (2019) Two decades of SPECT/CT - the coming of age of a technology: an updated review of literature evidence. Eur J Nucl Med Mol Imaging 46:1990–2012. https://doi.org/10.1007/s00259-019-04404-6
14. Hanson SK, Grotta JC, Rhoades H et al (1993) Value of single-photon emission-computed tomography in acute stroke therapeutic trials. Stroke 24:1322–1329. https://doi.org/10.1161/01.str.24.9.1322
15. Khalil MM, Tremoleda JL, Bayomy TB et al (2011) Molecular SPECT imaging: an overview. Int J Mol Imaging 2011:796025. https://doi.org/10.1155/2011/796025
16. Lu FM, Yuan Z (2015) PET/SPECT molecular imaging in clinical neuroscience: recent advances in the investigation of CNS diseases. Quant Imaging Med Surg 5:433–447. https://doi.org/10.3978/j.issn.2223-4292.2015.03.16
17. Son H, Jang K, Lee H et al (2019) Use of molecular imaging in clinical drug development: a systematic review. Nucl Med Mol Imaging 53:208–215. https://doi.org/10.1007/s13139-019-00593-y
18. Gudasheva TA, Voronina TA, Ostrovskaya RU et al (1996) Synthesis and antiamnesic activity of a series of N-acylprolyl-containing dipeptides. Eur J Med Chem 31:151–157. https://doi.org/10.1016/0223-5234(96)80448-X
19. Boiko SS, Ostrovskaya RU, Zherdev VP et al (2000) Pharmacokinetics of new nootropic acylprolyldipeptide and its penetration across the blood-brain barrier after oral administration. Bull Exp Biol Med 129:359–361. https://doi.org/10.1007/bf02439270
20. Vorobyov V, Kaptsov V, Kovalev G et al (2011) Effects of nootropics on the EEG in conscious rats and their modification by glutamatergic inhibitors. Brain Res Bull 85:123–132. https://doi.org/10.1016/j.brainresbull.2011.02.011
21. Neznamov GG, Teleshova ES (2009) Comparative studies of Noopept and piracetam in the treatment of patients with mild cognitive disorders in organic brain diseases of vascular and traumatic origin. Neurosci Behav Physiol 39:311–321. https://doi.org/10.1007/s11055-009-9128-4
22. Ramis-Ramos G (2003) Antioxidants|syntheyic antioxidants. In: Caballero B (ed) Encyclopedia of food science and nutrition, 2nd edn. Academic Press, Cambridge, pp 265–275. https://doi.org/10.1016/b0-12-227055-x/00054-7
23. Léveillé J, Demonceau G, De Roo M et al (1989) Characterization of technetium-99m-L, L-ECD for brain perfusion imaging, part 2: biodistribution and brain imaging in humans. J Nucl Med 30:1902–1910
24. Khater SI, El-Sharawy DM, El Refaye MS et al (2020) Optimization and tissue distribution of [^{125}I]iododomperidone as a

radiotracer for D2-receptor imaging. J Radioanal Nucl Chem 325:343–355. https://doi.org/10.1007/s10967-020-07236-z
25. Neirinckx RD, Canning LR, Piper IM et al (1987) Technetium-99m d, l-HM-PAO: a new radiopharmaceutical for SPECT imaging of regional cerebral blood perfusion. J Nucl Med 28:191–202
26. Henley JM, Wilkinson KA (2016) Synaptic AMPA receptor composition in development, plasticity and disease. Nat Rev Neurosci 17:337–350. https://doi.org/10.1038/nrn.2016.37
27. Abe H, Jitsuki S, Nakajima W et al (2018) CRMP2-binding compound, edonerpic maleate, accelerates motor function recovery from brain damage. Science 360:50–57. https://doi.org/10.1126/science.aao2300
28. Bailey A, Berwick DC, Camarini R et al (2022) Building bridges in neuropharmacology: new therapeutic approaches for psychiatric and neurodegenerative disorders. Br J Pharmacol 179:1475–1477. https://doi.org/10.1111/bph.15711
29. Astrup J, Siesjö BK, Symon L (1981) Thresholds in cerebral ischemia—the ischemic penumbra. Stroke 12:723–725. https://doi.org/10.1161/01.str.12.6.723
30. Boyko M, Gruenbaum SE, Gruenbaum BF et al (2014) Brain to blood glutamate scavenging as a novel therapeutic modality: a review. J Neural Transm (Vienna) 121:971–979. https://doi.org/10.1007/s00702-014-1181-7
31. Kett-White R, Hutchinson PJ, Al-Rawi PG et al (2002) Adverse cerebral events detected after subarachnoid hemorrhage using brain oxygen and microdialysis probes. Neurosurgery 50:1213–1221. https://doi.org/10.1097/00006123-200206000-00008
32. Song HC, Bom HS, Cho KH et al (2003) Prognostication of recovery in patients with acute ischemic stroke through the use of brain SPECT with Technetium-99m–labeled metronidazole. Stroke 34:982–986. https://doi.org/10.1161/01.Str.0000062902.94892.F5
33. Jingtao J, Sato S, Yamanaka N (1999) Changes in cerebral blood flow and blood brain barrier in the gerbil hippocampal CA1 region following repeated brief cerebral ischemia. Med Electron Microsc 32:175–183. https://doi.org/10.1007/s007950050025
34. Kolbaev SN, Sharonova IN, Skrebitsky VG (2021) Cellular and receptor mechanisms of action of nootropic and neuroprotective peptides used in clinical practice. Hum Physiol 47:870–877. https://doi.org/10.1134/s0362119721080077
35. Ostrovskaya RU, Gruden MA, Bobkova NA et al (2007) The nootropic and neuroprotective proline-containing dipeptide noopept restores spatial memory and increases immunoreactivity to amyloid in an Alzheimer's disease model. J Psychopharmacol 21:611–619. https://doi.org/10.1177/0269881106071335
36. Sanad MH, Marzook FA, Ibrahim IT et al (2023) Preparation and bioevaluation of radioiodinated omberacetam as a radiotracer for brain imaging. Radiochemistry 65:114–121. https://doi.org/10.1134/S1066362223010162
37. El-Kawy OA, García-Horsman JA (2017) ^{99m}Tc-labeled glimepiride as a tracer for targeting pancreatic β-cells mass: preparation and preclinical evaluation. J Radioanal Nucl Chem 314:2539–2550. https://doi.org/10.1007/s10967-017-5615-1
38. El-Kawy OA, Ibrahim IT, Farah K (2015) Technetium-99 m labeling and evaluation of olsalazine: a novel agent for ulcerative colitis imaging. J Label Compd Radiopharm 58:336–341. https://doi.org/10.1002/jlcr.3306
39. Sanad MH, Marzook EA, El-Kawy OA (2017) Radiochemical and biological characterization of ^{99m}Tc-oxiracetam as a model for brain imaging. Radiochemistry 59:624–629. https://doi.org/10.1134/S106636221706011X
40. Hsu KC, Chen YF, Lin SR et al (2011) iGEMDOCK: a graphical enviroment of enhanching GEMDOCK using pharmacological interactions and post-screening analysis. BMC Bioinform 12:S33. https://doi.org/10.1186/1471-2105-12-S1-S33
41. El-Kawy OA, Sayed MS, Abdel-Razek AS (2020) Preparation and evaluation of ^{99m}Tc-anidulafungin: a potential radiotracer for fungal infection. J Radioanal Nucl Chem 325:683–694. https://doi.org/10.1007/s10967-020-07274-7
42. El-Kawy OA, Farah K (2015) Radiocomplexation and biological evaluation of nemonoxacin in mice infected with multiresistant *Staphylococcus aureus* and penicillin-resistant Streptococci. J Radioanal Nucl Chem 306:123–130. https://doi.org/10.1007/s10967-015-4069-6
43. El-Kawy OA, García-Horsman JA (2017) ^{99m}Tc-roxifiban: a potential molecular imaging agent for the detection and localization of acute venous thrombosis. J Radioanal Nucl Chem 311:1719–1728. https://doi.org/10.1007/s10967-017-5183-4
44. El-Kawy OA, Talaat HM (2016) Preparation, characterization and evaluation of ^{186}Re-idarubicin: a novel agent for diagnosis and treatment of hepatocellular carcinoma. J Label Compd Radiopharm 59:72–77. https://doi.org/10.1002/jlcr.3368
45. El-Kawy OA, García-Horsman JA, Tuominen RK (2016) Labelling, molecular modelling and biological evaluation of vardenafil: a potential agent for diagnostic evaluation of erectile dysfunction. Appl Radiat Isot 118:258–265. https://doi.org/10.1016/j.apradiso.2016.09.023
46. Du Sert NP, Hurst V, Ahluwalia A et al (2020) The ARRIVE guidelines 2.0: updated guidelines for reporting animal research. Br J Pharmacol 177:3617–3624. https://doi.org/10.1111/bph.15193